ISSN 1070-3284, Russian Journal of Coordination Chemistry, 2018, Vol. 44, No. 8, pp. 518–531. © Pleiades Publishing, Ltd., 2018.
Original Russian Text © A.V. Ivanov, A.V. Gerasimenko, I.V. Egorova, A.S. Zaeva, E.V. Novikova, N.A. Rodionova, V. Gowda, O.N. Antzutkin, 2018, published in Koordinatsionnaya Khimiya, 2018, Vol. 44, No. 4, pp. 266–280.

Chemisorption Synthesis of the Ion-Polymeric Heteronuclear Gold(III)–Bismuth(III) Complex $([Au\{S_2CN(C_3H_7)_2\}_2]_3[Bi_2Cl_9])_n$ Based on $[Bi_2\{S_2CN(C_3H_7)_2\}_6]$: ^{13}C MAS NMR, Supramolecular Structure, and Thermal Behavior

A. V. Ivanov[a, *], A. V. Gerasimenko[b], I. V. Egorova[c], A. S. Zaeva[a], E. V. Novikova[a], N. A. Rodionova[c], V. Gowda[d, e], and O. N. Antzutkin[d, f]

[a] *Institute of Geology and Nature Management, Far East Branch, Russian Academy of Sciences, Blagoveshchensk, 675000 Russia*
[b] *Institute of Chemistry, Far East Branch, Russian Academy of Sciences, Vladivostok, 690022 Russia*
[c] *Blagoveshchensk State Pedagogical University, Blagoveshchensk, 675000 Russia*
[d] *Luleå University of Technology, SE-97187 Luleå, Sweden*
[e] *University of Oulu, P.O. Box 3000, FI-90014 Oulu, Finland*
[f] *Warwick University, Coventry CV4 7AL, United Kingdom*
**e-mail: alexander.v.ivanov@chemist.com*

Received September 28, 2017

Abstract—Chemisorption synthesis on the basis of the binuclear compound $[Bi_2\{S_2CN(C_3H_7)_2\}_6]$ (**I**) and preparative isolation of the ion-polymeric heteronuclear gold(III)–bismuth(III) complex $([Au\{S_2CN(C_3H_7)_2\}_2]_3[Bi_2Cl_9])_n$ (**II**) are carried out. Compounds **I** and **II** are characterized in comparison by IR spectroscopy and ^{13}C CP-MAS NMR. According to the X-ray diffraction analysis data (CIF file CCDC no. 1407705), the cationic moiety of compound **II** exhibits an unusually complicated supramolecular structure including six isomeric noncentrosymmetric complex cations $[Au\{S_2CN(C_3H_7)_2\}_2]^+$ (hereinafter A–F) and two binuclear anions $[Bi_2Cl_9]^{3-}$ as conformers. The isomeric gold(III) cations perform various structural functions. Owing to pair secondary interactions Au···S, cations B, C, E, and F form centrosymmetric ([E···E], [F···F]) and noncentrosymmetric ([B···C]) binuclear aggregates $[Au_2\{S_2CN(C_3H_7)_2\}_4]^{2+}$, whereas cations A and D are not involved in dimerization. The strongest secondary Au···S bonds are formed between the binuclear and mononuclear cations, resulting in the formation of supramolecular cation-cationic polymer chains of two types: $(\cdots A\cdots[B\cdots C]\cdots A\cdots[B\cdots C]\cdots)_n$ and $(D\cdots[E\cdots E]\cdots D\cdots[F\cdots F]\cdots])_n$. In both chains, the gold atoms of the binuclear cations are characterized by a distorted octahedral coordination $[S_6]$, whereas in the mononuclear cations the gold atoms retain the square environment $[S_4]$. The cation-anionic interactions are provided by secondary bonds Cl···S involving the terminal chlorine atoms of isomeric $[Bi_2Cl_9]^{3-}$ and the sulfur atoms of the binuclear cations $[Au_2\{S_2CN(C_3H_7)_2\}_4]^{2+}$. The character of the thermal behavior of compounds **I** and **II** is studied by simultaneous thermal analysis with the identification of intermediate and final products of the thermal transformations. The thermolysis of compound **I** at 193–320°C is accompanied by the formation of Bi_2S_3 with an impurity of reduced metallic bismuth particles. The final products of the thermal transformations of compound **II** are reduced elemental gold and Bi_2O_3, and the thermal transformation intermediates are $BiCl_3$ and Bi_2S_3.

Keywords: bismuth dithiocarbamates, gold(III) chemisorption, ion-polymeric gold(III)–bismuth complexes, crystal structure, supramolecular self-organization, secondary interactions Au···S

DOI: 10.1134/S1070328418080043

INTRODUCTION

Bismuth is a special element for several reasons. It was considered for a long time that in the periodic system bismuth completes the elements having stable nuclides. However, it has been shown rather recently (first theoretically [1] and then experimentally [2]) that bismuth presented in nature by the single nuclide ^{209}Bi is radioactive in fact due to the α-decay with the formation of the ^{205}Tl nucleus. Nevertheless, the half-life estimated as $1.9 \pm 0.2 \times 10^{19}$ years and exceeding the commonly accepted age of the Universe by nine orders of magnitude provides the radiation safety of

bismuth and its compounds. Difficulties of the experimental confirmation of ^{209}Bi radioactivity are related to a very low frequency of its nuclear decay and a low energy of the formed α particles. In addition, among heavy metals, bismuth is characterized by unusually low toxcity due to which bismuth is named "green metal". For this reason, there is tendency to replace lead and antimony by bismuth in industry (if possible). A low toxicity of the bismuth compounds, in particular, in the composition of the complexes (bismuth subsalicylate, subcitrate, and ethanediol) makes it possible to use them as the main components of drugs with antiulcerogenic, anti-inflammatory, and antibacterial (antispirochetic) effects. A broad range of high antitumor [3–8] and antibacterial activity [9–11] was found for the bismuth dithiocarbamate and dithiocarbamate halide complexes. In addition, bismuth dithiocarbamates are convenient precursors for the preparation of film and nanosized bismuth sulfides as a basis of semiconductor materials [12–17]. Intermolecular secondary interactions Bi···S play the determining role in the supramolecular self-organization of the bismuth(III) dithiocarbamate complexes [18–20].

We have previously synthesized and structurally characterized binuclear bismuth(III) dipropyldithiocarbamate $[Bi_2\{S_2CN(C_3H_7)_2\}_6]$ (**I**) [19] and two polymorphic modifications of bismuth(III) dibutyldithiocarbamate [20]. An unusually complicated supramolecular self-organization was established for compound **I**. Compound **I** includes six isomeric molecules $[Bi\{S_2CN(C_3H_7)_2\}_3]$ with the pentagonal bipyramidal structure, one of the axial positions of which is populated by a lone sterically directed electron pair of the central bismuth atom, and the pairs of secondary Bi···S bonds join the conformer molecules to form four types of isomeric binuclear molecules $[Bi_2\{S_2CN(C_3H_7)_2\}_6]$ (two centrosymmetric and two noncentrosymmetric in a ratio of 1 : 1 : 2 : 2). The second complex forms two polymorphic modifications, one of which is presented by the centrosymmetric binuclear molecule $[Bi_2\{S_2CN(C_4H_9)_2\}_6]$ [20, 21], and the structure of the second modification includes two isomeric noncentrosymmetric binuclear molecules [20]. In addition, the capability of binding gold(III) from solutions was found for compound **I**. The heteronuclear gold(III)–bismuth(III) complexes $[Au\{S_2CN(C_3H_7)_2\}_2]_3[Bi_3Cl_{12}]$ [22] and $[Au\{S_2CN(C_3H_7)_2\}_2]_3[Bi_2Cl_9] \cdot 1/2OC(CH_3)_2 \cdot 1/2HCl$ [23] were identified in the chemisorption systems.

Continuing these investigations, in this work we studied the thermal behavior and chemisorption activity of compound **I** toward a solution of $AuCl_3$ in 2 M HCl and preparatively isolated (as an individual form of gold(III) binding) ion-polymeric bis(*N*,*N*-dipropyldithiocarbamato-S,S')gold(III) nonachlorodibismuthate $[Au\{S_2CN(C_3H_7)_2\}_2]_3[Bi_2Cl_9]$ (**II**) (with the supramolecular structure basically different from the structure of the solvated form [23]) characterized by X-ray diffraction analysis, IR spectroscopy, ^{13}C CP-MAS NMR, and simultaneous thermal analysis (STA).

EXPERIMENTAL

The starting sodium *N*,*N*-dipropyldithiocarbamate, $Na\{S_2CN(C_3H_7)_2\} \cdot H_2O$ (**III**), was synthesized by the reaction of equimolar amounts of dipropylamine and carbon disulfide (Merck) in an alkaline medium [24].

IR for **III** (KBr), ν, cm^{-1}: 3368 s.br, 2963 m, 2930 m, 2872 m, 2130 s, 1632 s, 1468 s, 1408 s, 1368 s, 1304 m, 1298 m, 1267 m, 1237 s, 1198 s, 1138 s, 1107 w, 1088 m, 1028 m, 970 s, 891 m, 864 m, 745 m, 602 w, 536 w. ^{13}C CP-MAS NMR (δ, ppm): 208.3 ($-S_2CN=$); 59.4, 57.9 (1 : 1, $=NCH_2-$); 22.3, 21.5 (1 : 1, $-CH_2-$); 12.6, 11.5 (1 : 1, $-CH_3$) [19].

Synthesis of compound I was carried out by the reaction of an aqueous solution of $Bi(NO_3)_3 \cdot 5H_2O$ (predissolved in a minor amount of HNO_3) and an aqueous solution of compound **III** taken in a superstoichiometric (~15%) ratio. A bulky precipitate formed was separated and washed with water on the filter. Lustrous yellow needle-like crystals of compound **I** were obtained by crystallization from acetone, mp = 152–155°C.

IR for **I** (KBr), ν, cm^{-1}: 2961 s, 2928 m, 2871 m, 1487 s, 1476 s, 1420 s, 1364 m, 1304 m, 1271 w, 1235 s, 1196 m, 1144 s, 1102 m, 1086 m, 963 m, 891 m, 770 w, 748 m, 602 m, 536 w.

^{13}C CP-MAS NMR (δ, ppm): 203.6, 202.1, 200.9, 200.1 (6 : 5 : 4 : 3, $-S_2CN=$); 56.6, 56.1, 55.3 (3 : 2 : 1, $=NCH_2-$); 23.0, 21.6, 21.3, 20.9, 20.6, 20.1 (1 : 6 : 5 : 12 : 4 : 8, $-CH_2-$); 13.2, 13.0, 12.7, 12.3, 12.2, 11.8, 11.6 (1 : 5 : 7 : 4 : 7 : 6 : 6, $-CH_3$) [19].

Synthesis of compound II. A solution (20 mL) of $AuCl_3$ in 2 M HCl containing 58.7 mg (0.2980 mmol) of gold was gradually added with stirring (1 h) to compound **I** (150 mg, 0.1016 mmol). The heterogeneous reaction of gold(III) binding from a solution by the freshly precipitated binuclear bismuth complex (chemisorbent **I**) can be presented as follows:

$$[Bi_2\{S_2CN(C_3H_7)_2\}_6] + 3H[AuCl_4] = [Au\{S_2CN(C_3H_7)_2\}_2]_3[Bi_2Cl_9] + 3HCl.$$

The residual content of gold in the solution was determined on a Hitachi atomic absorption spectrometer (1 class, model 180-50). The established degree of binding of gold by complex **I** was 98.7%.

The chemisorption of gold(III) is accompanied by a gradual change in the color of the starting complex-sorbent from lemon-yellow to bright orange with the simultaneous decoloration of the working solution, indicating a change in the chemical composition of the solid phase and the formation of new compounds. At

the completion of the process, the formed bright orange precipitate was filtered off, washed with water, dried on the filter, and dissolved in an acetone–ethanol (1 : 1) mixture. Transparent orange prismatic crystals of compound **II** for the diffractometric experiment were obtained by the slow evaporation of the solvents at ambient temperature.

IR (KBr), ν, cm^{-1}: 2963 s, 2930 m, 2871 m, 1551 s, 1491 s, 1464 m, 1431 s, 1364 m, 1343 m, 1304 m, 1242 s, 1190 m, 1148 s, 1104 w, 1086 m, 961 m, 895 m, 766 w, 750 m, 602 m, 536 w. ^{13}C CP-MAS NMR (δ, ppm): 201.5, 199.6, 198.4, 197.0, 196.4, 195.4, 194.0, 192.6, 191.0 (1 : 1 : 1 : 2 : 1 : 1 : 2 : 2 : 1, $-S_2CN=$); 58.6, 57.9, 57.0, 56.2, 55.3, 53.7, 50.4 ($=NCH_2-$); 23.8, 22.0, 21.8, 21.5 ($-CH_2-$); 14.3, 13.8, 13.4, 13.1, 13.0, 12.6, 12.2, 12.0, 11.6, 11.2 ($-CH_3$).

^{13}C CP-MAS NMR spectra were recorded on a CMX-360 pulse spectrometer (Agilent/Varian/Chemagnetics InfinityPlus) with a working frequency of 90.52 MHz, a superconducting magnet (B_0 = 8.46 T), and Fourier transform. Cross-polarization (CP) from protons was used for spectra recording, and the $^{13}C-^{1}H$ proton decoupling with a radiofrequency field at the resonance frequency of protons was used to suppress dipole–dipole interactions [25]. For ^{13}C NMR measurements, complexes **I** and **II** (~80 mg) were placed in rotors of ZrO_2 ceramics with a diameter of 4.0 mm. Rotation at a magic angle was conducted at a frequency of 5200 or 5300(1) Hz (scan number 4000 or 16800, duration of proton π/2 pulses 3.3 or 5.0 μs, $^{1}H-^{13}C$ contact time 2.5 or 2.5 ms, and recycling delays 3.0 s for complexes **I** and **II**, respectively). The ^{13}C NMR isotropic chemical shifts are given relative to one of the components of crystalline adamantane (δ = 38.48 ppm relative to $Si(CH_3)_4$). The homogeneity of the magnetic field was monitored by the width (2.6 Hz) of the reference line of adamantane. Chemical shifts are given with a correction of the drift of the magnetic field during experiments, the frequency equivalent of which for ^{13}C nuclei was 0.098 Hz/h.

The IR spectra of the complexes in KBr pellets were recorded on an FSM-1201 interferential FT-IR spectrometer in a range of 400–4000 cm^{-1}. The instrument was controlled and the spectra were processed using the FSpec program (version 4.0.0.2 for Windows, OOO Monitoring, Russia).

X-ray diffraction analysis of compound II was carried out from a flat prismatic single crystal on a BRUKER Kappa APEX II diffractometer (MoK_α radiation, λ = 0.71073 Å, graphite monochromator) at 170(2) K. An X-ray absorption correction for a sample of compound **II** was applied by indices of single crystal faces. The structure was determined by a direct method and refined by least squares in the anisotropic approximation for Au, Bi, Cl, and S atoms. Since the quality of the single crystals was low, a number of carbon atoms in the alkyl substituents of the PDtc ligands in the composition of the isomeric complex gold(III) cations, namely, Au(2)–C(25); Au(3)–C(41), C(42); Au(4)–C(52), C(53), C(55), C(56); and Au(5)–C(62), C(63) was not localized and was not involved in refinement. The localized carbon and nitrogen atoms were refined isotropically. The positions of hydrogen atoms were calculated geometrically and included in refinement by the riding model. Data were collected and edited and the unit cell parameters were refined using the APEX2 program packages [26]. All calculations on structure determination and refinement were performed using the SHELXTL/PC program packages [27].

The main crystallographic data and results for structure refinement are presented in Table 1. Selected bond lengths and angles are given in Table 2.

The coordinates of atoms, bond lengths, bond angles, and temperature parameters for the structure of compound **II** were deposited with the Cambridge Crystallographic Data Centre (CIF file CCDC no. 1407705; deposit@ccdc.cam.ac.uk or http://www.ccdc.cam.ac.uk).

Thermal behavior of compounds I and II was studied by the STA method with the simultaneous detection of thermogravimetry (TG) and differential scanning calorimetry (DSC) curves. The study was conducted on an STA 449C Jupiter instrument (NETZSCH) in corundum crucibles under a cap with a hole providing the vapor pressure during thermolysis equal to 1 atm. The heating rate was 5°C/min to 550 and 1100°C under an argon atmosphere. The weighed samples were 2.980–7.203 (**I**) and 2.014–7.445 mg (**II**), the accuracy of temperature measurements was ±0.7°C, and the accuracy of mass change was $\pm 1 \times 10^{-4}$ mg. After the thermal analysis of compound **I**, the residual substance was examined on a JSM 6390LV JEOL scanning electron microscope (Japan) equipped with the Oxford INCA Energy 350-Wave microanalysis system (England) with energy and wavelength dispersion. The qualitative determination of the chemical composition was carried out by the microprobe method using an energy dispersive spectrometer.

RESULTS AND DISCUSSION

The IR spectra of compounds **I–III** exhibit bands assigned to ligands PDtc. The bands of alkyl groups lie in a range of 2963–2871 cm^{-1}. The spectra of all the three compounds in a range of 1551–1468 cm^{-1} contain an intense band caused by the C–N bond stretching vibrations in the dithiocarbamate groups $=NC(S)S-$ [24]. The experimental ν(C–N) values for them are intermediate between the values of stretching vibrations of the ordinary C–N (1360–1250 cm^{-1}) and double C=N (1690–1640 cm^{-1}) bonds [28], which reflects the partially double character of the N–C(S)S bonds. The high value of ν(C–N) (1551 cm^{-1}) in the IR spectrum of compound **II** indicates that the

Table 1. Crystallographic data and experimental and refinement parameters for the structure of compound $[Au\{S_2CN(C_3H_7)_2\}_2]_3[Bi_2Cl_9]$ (**II**)

Parameter	Value
Empirical formula	$C_{42}H_{84}N_6S_{12}Cl_9Au_3Bi_2$
FW	2385.78
Crystal system	Orthorhombic
Space group	*Pbca*
a, Å	34.222(3)
b, Å	23.542(2)
c, Å	37.139(3)
V, Å^3	29921(5)
Z	16
ρ_{calcd}, g/cm^3	2.118
μ, mm^{-1}	11.242
F(000)	18016
Crystal size, mm	0.25 × 0.22 × 0.06
Range of data collection over θ, deg	1.19–25.4
Ranges of reflection indices	$-41 \le h \le 41$, $-28 \le k \le 28$, $-38 \le l \le 44$
Measured reflections	390590
Independent reflections (R_{int})	26709 (0.1217)
Reflections with $I > 2\sigma(I)$	19873
Refinement parameters	836
GOOF	1.059
R factors for $F^2 > 2\sigma(F^2)$	$R_1 = 0.0884$, $wR_2 = 0.2037$
R factors for all reflections	$R_1 = 0.1199$, $wR_2 = 0.2243$
Residual electron density (min/max), *e*/Å^3	−3.147/9.262

strength of the C–N(S)S bonds increases due to the redistribution of ligands PDtc to the internal sphere of gold when the heteronuclear Au(III)–Bi(III) complex is formed. The doublet splitting of the ν(C–N) band (1487 and 1476 cm^{-1}) appears in the IR spectrum of the starting complex **I**, which can be explained by different degrees of degeneracy of vibrations of the bond discussed. In addition, ranges of 1148–1138 and 970–961 cm^{-1} in the experimental IR spectra exhibit bands caused by asymmetric and symmetric stretching vibrations, respectively, of the –C(S)S– groups of ligands PDtc [24, 29].

The experimental ^{13}C CP-MAS NMR spectra of polycrystalline samples of the complexes under study (Fig. 1) contain resonance signals of ligands PDtc in the chemical groups: =NC(S)S–, =NCH$_2$–, –CH$_2$–, and –CH$_3$. The range of =NC(S)S– groups of complexes **I** and **II** is most informative in structural respect and exhibits four and nine ^{13}C resonance signals, respectively. As compared to the starting sodium salt **III** (δ(^{13}C) 208.3 ppm), the ^{13}C chemical shifts of the dithiocarbamate groups in compounds **I** and **II** are characterized by substantially lower values and lie in the ranges 203.6–200.1 and 201.5–191.0 ppm, respectively. The effect observed is explained by an increase in electronic shielding of the carbon nuclei of the =NC(S)S– groups due to their covalent bonding by the bismuth and gold atoms. Since the chemical affinity to sulfur of the latter is high, the electronic system of gold is more efficiently involved in the additional shielding of carbon of the =NC(S)S– groups. The ratios of integral intensities in the discussed groups of signals close to 6 : 5 : 4 : 3 (Fig. 1a) and 1 : 1 : 1 : 2 : 1 : 1 : 2 : 2 : 1 (Fig. 1b) indicate that the obtained complexes contain 18 (**I**) and 12 (**II**) structurally nonequivalent ligands, reflecting a complicated character of their structural organization.

Before discussing the structure of compound **II**, let us consider the correspondence of the data of IR spectroscopy, ^{13}C CP-MAS NMR, and X-ray diffraction analysis for compounds **I** and **II**. As expected from the ^{13}C CP-MAS NMR data, the structure of compound **I** including six isomeric molecules $[Bi\{S_2CN(C_3H_7)_2\}_3]$ contains 18 nonequivalent PDtc ligands. The cationic moiety of compound **II** presented by six noncentrosymmetric complex ions $[Au\{S_2CN(C_3H_7)_2\}_2]^+$ (Figs. 2a, 3; Table 2) has 12 nonequivalent ligands on the whole. The conclusion from the data on IR spectroscopy about stronger N–C(S)S bonds in complex **II** compared to complex **I** is also confirmed by the X-ray diffraction analysis: four of the discussed bonds in the structure of complex **II** (1.283, 1.288, 1.300, and 1.303 Å, Table 2) are noticeably shorter than the shortest bond in compound **I** (1.308–1.387 Å [19]).

The crystal and supramolecular structures of the ion-polymeric heteronuclear complex Au(III)–Bi(III) was determined by X-ray diffraction analysis. The unit cell of complex **II** contains 16 formula units $[Au\{S_2CN(C_3H_7)_2\}_2]_3[Bi_2Cl_9]$. The cationic moiety of the complex includes six structurally nonequivalent noncentrosymmetric ions $[Au\{S_2CN(C_3H_7)_2\}_2]^+$: hereinafter cations A with atom Au(1), B with Au(2), C with Au(3), D with Au(4), E with Au(5), and F with Au(6) (Fig. 2a, Table 2). The anionic moiety is presented by two nonequivalent noncentrosymmetric binuclear complex ions $[Bi_2Cl_9]^{3-}$ including pairs of atoms Bi(1), Bi(2) and Bi(3), Bi(4) (Figs. 2b, 2c). The interatomic Bi(1)–Bi(2) (3.9744(5) Å) and Bi(3)–Bi(4) (3.9636(5) Å) distances in the anions discussed are consistent with the published data [30–32]. The bismuth atoms are located in the distorted octahedral environment of six chlorine atoms, three of which (terminal) are bound more strongly by the central bismuth

Table 2. Bond lengths (*d*, Å) and bond angles (ω, deg) in the structure of compound **II***

Bond	*d*, Å	Bond	*d*, Å
Isomeric cations $[Au\{S_2CN(C_3H_7)_2\}_2]^+$			
Au(1)–S(1)	2.346(3)	S(2)–C(1)	1.656(9)
Au(1)–S(2)	2.310(2)	S(3)–C(8)	1.692(9)
Au(1)–S(3)	2.328(2)	S(4)–C(8)	1.751(9)
Au(1)–S(4)	2.325(3)	N(1)–C(1)	1.338(11)
S(1)–C(1)	1.756(9)	N(2)–C(8)	1.325(11)
Au(2)–S(5)	2.330(2)	S(5)–C(15)	1.754(8)
Au(2)–S(6)	2.346(2)	S(6)–C(15)	1.746(8)
Au(2)–S(7)	2.337(2)	S(7)–C(22)	1.761(9)
Au(2)–S(8)	2.333(2)	S(8)–C(22)	1.741(9)
Au(2)···S(1)	3.331(3)	N(3)–C(15)	1.303(10)
Au(2)···S(9)[a]	3.352(2)	N(4)–C(22)	1.288(10)
Au(3)–S(9)	2.342(2)	S(9)–C(29)	1.686(8)
Au(3)–S(10)	2.339(2)	S(10)–C(29)	1.646(8)
Au(3)–S(11)	2.337(2)	S(11)–C(36)	1.709(9)
Au(3)–S(12)	2.342(2)	S(12)–C(36)	1.731(9)
Au(3)···S(2)	3.342(3)	N(5)–C(29)	1.452(10)
Au(3)···S(7)[b]	3.591(3)	N(6)–C(36)	1.312(13)
Au(4)–S(13)	2.312(3)	S(14)–C(43)	1.685(10)
Au(4)–S(14)	2.305(2)	S(15)–C(50)	1.708(13)
Au(4)–S(15)	2.316(4)	S(16)–C(50)	1.627(13)
Au(4)–S(16)	2.354(3)	N(7)–C(43)	1.357(12)
S(13)–C(43)	1.728(10)	N(8)–C(50)	1.342(15)
Au(5)–S(17)	2.337(2)	S(17)–C(57)	1.625(14)
Au(5)–S(18)	2.341(3)	S(18)–C(57)	1.715(14)
Au(5)–S(19)	2.331(2)	S(19)–C(64)	1.724(10)
Au(5)–S(20)	2.345(3)	S(20)–C(64)	1.729(10)
Au(5)···S(15)	3.417(4)	N(9)–C(57)	1.408(16)
Au(5)···S(17)[c]	3.513(3)	N(10)–C(64)	1.300(12)
Au(6)–S(21)	2.345(2)	S(21)–C(71)	1.742(9)
Au(6)–S(22)	2.327(2)	S(22)–C(71)	1.731(9)
Au(6)–S(23)	2.332(2)	S(23)–C(78)	1.737(12)
Au(6)–S(24)	2.322(2)	S(24)–C(78)	1.670(11)
Au(6)···S(16)	3.321(3)	N(11)–C(71)	1.283(11)
Au(6)···S(24)[d]	3.599(3)	N(12)–C(78)	1.362(14)
Isomeric anions $[Bi_2Cl_9]^{3-}$			
Bi(1)–Cl(1)	2.890(2)	Bi(2)–Cl(1)	2.901(2)
Bi(1)–Cl(2)	2.945(2)	Bi(2)–Cl(2)	3.039(2)
Bi(1)–Cl(3)	2.866(2)	Bi(2)–Cl(3)	2.890(2)
Bi(1)–Cl(4)	2.590(3)	Bi(2)–Cl(7)	2.581(3)
Bi(1)–Cl(5)	2.566(2)	Bi(2)–Cl(8)	2.558(3)
Bi(1)–Cl(6)	2.588(2)	Bi(2)–Cl(9)	2.546(2)
Cl(6)···S(12)[e]	3.334(3)	Cl(8)···S(8)[f]	3.373(3)
Cl(7)···S(5)[f]	3.394(3)	Cl(9)···S(8)[f]	3.541(3)
Bi(3)–Cl(10)	2.820(2)	Bi(4)–Cl(10)	2.938(2)
Bi(3)–Cl(11)	2.904(2)	Bi(4)–Cl(11)	2.858(2)
Bi(3)–Cl(12)	2.926(2)	Bi(4)–Cl(12)	3.080(2)
Bi(3)–Cl(13)	2.550(2)	Bi(4)–Cl(16)	2.567(3)
Bi(3)–Cl(14)	2.610(2)	Bi(4)–Cl(17)	2.538(3)
Bi(3)–Cl(15)	2.589(3)	Bi(4)–Cl(18)	2.533(2)
Cl(14)···S(20)[g]	3.339(4)	Cl(17)···S(23)[h]	3.512(3)
Cl(16)···S(22)[h]	3.434(3)	Cl(18)···S(24)[i]	3.530(3)

Таблица 2. (Contd.)

Angle	ω, deg	Angle	ω, deg
Isomeric cations $[Au\{S_2CN(C_3H_7)_2\}_2]^+$			
S(1)Au(1)S(2)	74.59(9)	C(1)S(1)Au(1)	85.1(3)
S(1)Au(1)S(3)	104.36(10)	C(1)S(2)Au(1)	88.5(3)
S(1)Au(1)S(4)	176.79(11)	C(8)S(3)Au(1)	87.0(3)
S(2)Au(1)S(3)	178.74(10)	C(8)S(4)Au(1)	85.8(3)
S(2)Au(1)S(4)	105.61(9)	S(1)C(1)S(2)	111.5(5)
S(3)Au(1)S(4)	75.48(9)	S(3)C(8)S(4)	111.6(5)
S(5)Au(2)S(6)	75.71(7)	C(15)S(5)Au(2)	87.2(3)
S(5)Au(2)S(7)	177.15(8)	C(15)S(6)Au(2)	86.8(3)
S(5)Au(2)S(8)	103.49(7)	C(22)S(7)Au(2)	87.5(3)
S(6)Au(2)S(7)	105.42(7)	C(22)S(8)Au(2)	88.1(3)
S(6)Au(2)S(8)	176.15(9)	S(5)C(15)S(6)	110.1(4)
S(7)Au(2)S(8)	75.20(7)	S(7)C(22)S(8)	108.9(5)
S(9)Au(3)S(10)	74.98(7)	C(29)S(9)Au(3)	83.0(3)
S(9)Au(3)S(11)	103.60(7)	C(29)S(10)Au(3)	83.9(3)
S(9)Au(3)S(12)	178.83(8)	C(36)S(11)Au(3)	86.5(3)
S(10)Au(3)S(11)	177.07(9)	C(36)S(12)Au(3)	85.9(3)
S(10)Au(3)S(12)	106.17(8)	S(9)C(29)S(10)	117.5(5)
S(11)Au(3)S(12)	75.24(7)	S(11)C(36)S(12)	112.3(5)
S(13)Au(4)S(14)	75.45(11)	C(43)S(13)Au(4)	85.7(4)
S(13)Au(4)S(15)	104.95(13)	C(43)S(14)Au(4)	86.9(3)
S(13)Au(4)S(16)	178.85(13)	C(50)S(15)Au(4)	84.2(4)
S(14)Au(4)S(15)	176.60(13)	C(50)S(16)Au(4)	84.7(4)
S(14)Au(4)S(16)	104.94(10)	S(13)C(43)S(14)	111.8(6)
S(15)Au(4)S(16)	74.73(13)	S(15)C(50)S(16)	116.4(7)
S(17)Au(5)S(18)	75.10(10)	C(57)S(17)Au(5)	84.8(5)
S(17)Au(5)S(19)	103.93(8)178.00(12)	C(57)S(18)Au(5)	82.8(5)
S(17)Au(5)S(20)	178.42(11)	C(64)S(19)Au(5)	86.5(3)
S(18)Au(5)S(19)	105.57(10)	C(64)S(20)Au(5)	86.0(3)
S(18)Au(5)S(20)	75.36(9)	S(17)C(57)S(18)	117.2(8)
S(19)Au(5)S(20)		S(19)C(64)S(20)	111.7(6)
S(21)Au(6)S(22)	75.18(8)	C(71)S(21)Au(6)	86.9(3)
S(21)Au(6)S(23)	178.53(10)	C(71)S(22)Au(6)	87.7(3)
S(21)Au(6)S(24)	105.21(8)	C(78)S(23)Au(6)	84.5(4)
S(22)Au(6)S(23)	103.99(8)	C(78)S(24)Au(6)	86.3(4)
S(22)Au(6)S(24)	178.55(10)	S(21)C(71)S(22)	110.3(5)
S(23)Au(6)S(24)	75.59(8)	S(23)C(78)S(24)	113.7(7)
Isomeric anions $[Bi_2Cl_9]^{3-}$			
Cl(1)Bi(1)Cl(2)	78.65(7)	Cl(1)Bi(2)Cl(7)	92.76(7)
Cl(1)Bi(1)Cl(3)	82.69(5)	Cl(1)Bi(2)Cl(8)	172.65(7)
Cl(1)Bi(1)Cl(4)	88.74(8)	Cl(1)Bi(2)Cl(9)	92.82(7)
Cl(1)Bi(1)Cl(5)	173.23(7)	Cl(2)Bi(2)Cl(3)	74.68(6)
Cl(1)Bi(1)Cl(6)	95.22(6)	Cl(2)Bi(2)Cl(7)	99.49(7)
Cl(2)Bi(1)Cl(3)	76.50(6)	Cl(2)Bi(2)Cl(8)	96.14(7)
Cl(2)Bi(1)Cl(4)	162.61(7)	Cl(2)Bi(2)Cl(9)	164.54(7)
Cl(2)Bi(1)Cl(5)	98.64(8)	Cl(3)Bi(2)Cl(7)	172.93(6)
Cl(2)Bi(1)Cl(6)	97.12(7)	Cl(3)Bi(2)Cl(8)	93.69(7)
Cl(3)Bi(1)Cl(4)	90.16(7)	Cl(3)Bi(2)Cl(9)	92.61(7)
Cl(3)Bi(1)Cl(5)	90.65(6)	Cl(7)Bi(2)Cl(8)	90.91(9)
Cl(3)Bi(1)Cl(6)	173.55(7)	Cl(7)Bi(2)Cl(9)	92.49(7)
Cl(4)Bi(1)Cl(5)	92.54(9)	Cl(8)Bi(2)Cl(9)	93.39(7)
Cl(4)Bi(1)Cl(6)	95.91(8)	Bi(1)Cl(1)Bi(2)	86.68(6)
Cl(5)Bi(1)Cl(6)	91.26(7)	Bi(1)Cl(2)Bi(2)	83.22(6)
Cl(1)Bi(2)Cl(2)	76.97(6)	Bi(1)Cl(3)Bi(2)	87.33(5)
Cl(1)Bi(2)Cl(3)	82.09(6)		

Таблица 2. (Contd.)

Angle	ω, deg	Angle	ω, deg
Cl(10)Bi(3)Cl(11)	82.69(6)	Cl(10)Bi(4)Cl(16)	98.55(8)
Cl(10)Bi(3)Cl(12)	80.28(7)	Cl(10)Bi(4)Cl(17)	168.48(7)
Cl(10)Bi(3)Cl(13)	90.37(7)	Cl(10)Bi(4)Cl(18)	91.23(7)
Cl(10)Bi(3)Cl(14)	175.05(9)	Cl(11)Bi(4)Cl(12)	75.38(6)
Cl(10)Bi(3)Cl(15)	89.63(8)	Cl(11)Bi(4)Cl(16)	173.30(7)
Cl(11)Bi(3)Cl(12)	77.13(6)	Cl(11)Bi(4)Cl(17)	87.45(8)
Cl(11)Bi(3)Cl(13)	171.71(7)	Cl(11)Bi(4)Cl(18)	93.64(7)
Cl(11)Bi(3)Cl(14)	95.44(7)	Cl(12)Bi(4)Cl(16)	98.08(7)
Cl(11)Bi(3)Cl(15)	89.55(8)	Cl(12)Bi(4)Cl(17)	98.35(7)
Cl(12)Bi(3)Cl(13)	97.28(8)	Cl(12)Bi(4)Cl(18)	164.10(7)
Cl(12)Bi(3)Cl(14)	94.85(9)	Cl(16)Bi(4)Cl(17)	92.13(9)
Cl(12)Bi(3)Cl(15)	164.15(7)	Cl(16)Bi(4)Cl(18)	93.06(8)
Cl(13)Bi(3)Cl(14)	91.11(8)	Cl(17)Bi(4)Cl(18)	92.51(8)
Cl(13)Bi(3)Cl(15)	94.97(10)	Bi(3)Cl(10)Bi(4)	86.97(6)
Cl(14)Bi(3)Cl(15)	94.94(10)	Bi(3)Cl(11)Bi(4)	86.94(5)
Cl(10)Bi(4)Cl(11)	81.44(6)	Bi(3)Cl(12)Bi(4)	82.55(6)
Cl(10)Bi(4)Cl(12)	75.97(6)		

* Symmetry transforms: [a] $-x + 3/2, y + 1/2, z$; [b] $-x + 3/2, y - 1/2, z$; [c] $x, -y + 1, -z$; [d] $-x, -y + 2, -z$; [e] $-1/2 + x, -1 + y, 1/2 - z$; [f] $1/2 - x, -1/2 + y, z$; [g] $1 + x, 3/2 - y, 1/2 + z$; [h] $1/2 - x, 2 - y, 1/2 + z$; [h] $1/2 + x, y, 1/2 - z$.

atom (Bi–Cl 2.533–2.610 Å) compared to three other atoms performing the μ_2-bridging function (Bi–Cl 2.820–3.080 Å). The latter are involved in joining the octahedra formed into the binuclear complex anion through the common face.

In all complex cations $[Au\{S_2CN(C_3H_7)_2\}_2]^+$, the coordination of the PDtc ligands is close to the isobidentate one (Au–S 2.305–2.354 Å) and results in the formation of two four-membered metallocycles $[AuS_2C]$ with the common gold atom. Small cycles are characterized by the distances Au···C (2.714–2.865 Å) and S···S (2.821–2.870 Å) significantly shorter than the sums of the van der Waals radii of the corresponding pairs of atoms (3.36 and 3.60 Å) [33]. The AuSSC and SAuCS torsion angles deviate from 180°. This effect is most pronounced for cation C: 170.99° and −172.56°, respectively. Thus, the atoms in the cycles discussed are not quite coplanar. On the contrary, in the $[AuS_4]$ chromophores, the SAuS diagonal angles are close to 180°, which indicates their square structure caused by the low-spin inner-orbital dsp^2-hybrid state of gold(III).

In the $C_2NC(S)S$ groups, the deviation of the atoms from the mean plane is fairly low and is most pronounced for the C(33) and C(40) atoms in cation C and the C(58) and C(68) atoms in E. The corresponding torsion angles SCNC are as follows: S(9)C(29)N(5)C(33) 19(1)°, S(10)C(29)N(5)C(33) 175.0(6)°, S(11)C(36)N(6)C(40) −158.2(7)°, S(12)C(36)N(6)C(40) 21(1)°; S(17)C(57)N(9)C(58) −161.8(8)°, S(18)C(57)N(9)C(58) 20(2)°, S(19)-C(64)N(10)C(68) 159.2(6)°, and S(20)-C(64)N(10)C(68) −22.(1)°. The contribution of double bonding to the formally ordinary bonds N–C(S)S provides their higher strength (1.283–1.452 Å) compared to the $N-CH_2$ bonds (1.420–1.674 Å), which is based on admixing of sp^2 to the sp^3-hybrid state of the nitrogen and carbon atoms due to the mesomeric effect of the dithiocarbamate groups.

In spite of the same building character of six nonequivalent gold(III) cations, they perform different structural functions in the structure of compound **II** and exhibit, as two bismuth(III) anions, reliable differences in lengths of the corresponding bonds (Au–S, C–S, N–C(S)S, Bi–Cl) and values of bond (SAuS, SCS, ClBiCl) and torsion angles (SCNC), which makes it possible to classify the discussed complex ions as conformational isomers.

The secondary bonds Au···S[1] of the nonvalent type between the isomeric gold(III) cations play the determining role in the supramolecular self-organization of complex **II**. Cations E and F participate in the formation of centrosymmetric binuclear aggregates [E···E] (interatomic distance Au(5)–Au(5)[c] in the dimer is 4.4288(10) Å) and [F···F] (Au(6)–Au(6)[d] 3.8079(8) Å) of the composition $[Au_2\{S_2CN(C_3H_7)_2\}_4]^{2+}$ due to pairs of symmetric secondary bonds Au(5)···S(17)[c] and Au(5)[c]···S(17) (3.513 Å), Au(6)···S(24)[d] and Au(6)[d]···S(24) (3.599 Å) (Fig. 2d). Nonsymmetric secondary bonds Au(3)···S(7)[b] (3.591 Å) and Au(2)[b]···S(9) (3.352 Å) occur between cations B and

[1] The concept of secondary bonds was proposed [34] for the description of interactions characterized by the distances comparable with the sums of the van der Waals radii of the corresponding atoms.

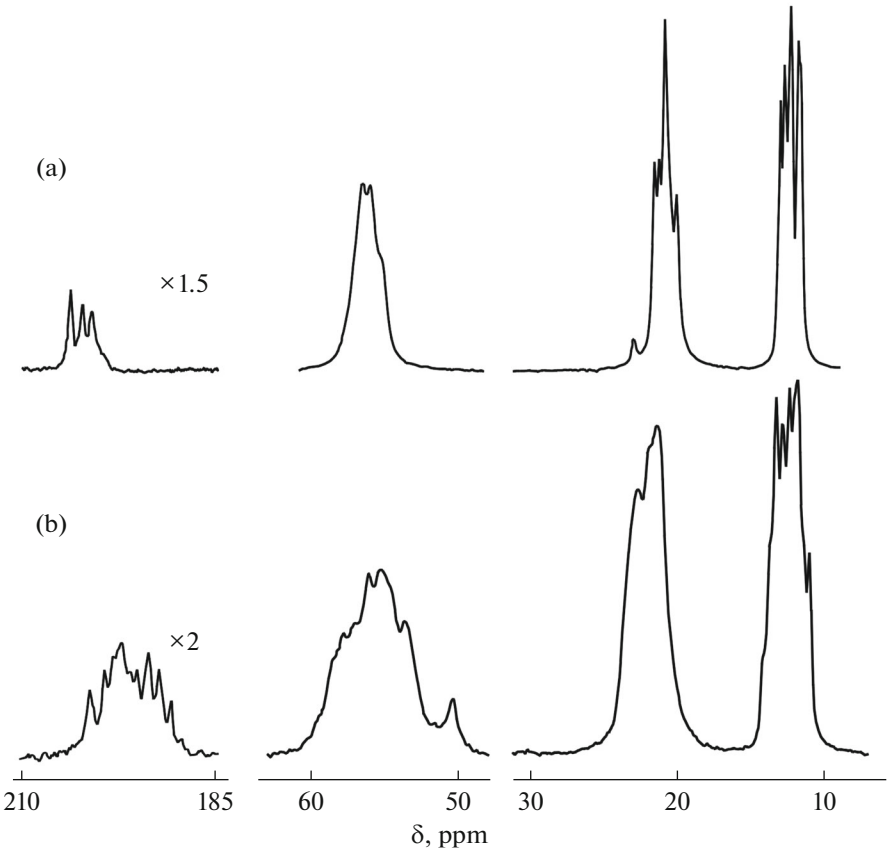

Fig. 1. ^{13}C CP-MAS NMR spectra of polycrystalline samples of compounds (a) **I** and (b) **II**. The scan number was (a) 4000 and (b) 16800, and the rotation frequency was (a) 5200 and (b) 5300 Hz.

C, resulting in the formation of noncentrosymmetric binuclear cations [B···C] (Au(2)–Au(3)[a] 4.1071(5) Å) (Fig. 3a). In the binuclear cations discussed, the planes of the $[AuS_4]$ chromophores are parallel (at the antiparallel orientations of the $[Au\{S_2CN(C_3H_7)_2\}_2]^+$ cations in the centrosymmetric dimers [E···E] and [F···F], Fig. 2d) but are somewhat shifted relative to each other along the bisectoral axes C–Au–C. The latter fact makes it possible to form stronger intercationic secondary bonds Au···S but results in an increase in the Au–Au interatomic distances. The different characters of the mutual steric orientation of the alkyl substituents in the mononuclear and binuclear gold(III) cations should also be mentioned. In the first case, the substituents are arranged both above and under the plane of the $[AuS_4]$ chromophore (Fig. 2a). In the second case, they are arranged at one side of the $[AuS_4]$ plane for each cation and are characterized by the mutually opposite directions (Fig. 2d) due to the efficient manifestation of interligand repulsion forces.

However, the strongest secondary Au···S bonds take place between the binuclear $[Au_2\{S_2CN(C_3H_7)_2\}_4]^{2+}$ and mononuclear $[Au\{S_2CN(C_3H_7)_2\}_2]^+$ cations (A and D, which are not in the composition of the binuclear aggregates). The former participate in the discussed interactions due to the gold atoms, and the latter present the both sulfur atoms of one of the PDtc ligands (Fig. 3). Mononuclear cations A form bonds only with the noncentrosymmetric binuclear cations [B···C] (Au(2)···S(1) (3.331 Å) and Au(3)···S(2) (3.342 Å)), whereas cations D interact with two centrosymmetric cations [E···E] and [F···F] (Au(5)···S(15) (3.417 Å) and Au(6)···S(16) (3.321 Å)). The sum of the van der Waals radii of gold and sulfur atoms is 3.46 Å [33]. Thus, the structure of compound **II** includes independent zigzag cation-cationic polymer chains orientated along the *y* axis of two types (Fig. 3): (a) $(\cdots A\cdots[B\cdots C]\cdots A\cdots[B\cdots C]\cdots)_n$ (angles Au(1)Au(2)Au(3)[a] 122.301(11)°, Au(2)[b]Au(3)Au(1) 116.483(11)°, Au(3)Au(1)Au(2) 141.961(10)°; interatomic distances Au(1)–Au(2) 4.6697(6) Å and Au(1)–Au(3) 4.6279(6) Å) and (b) $(\cdots D\cdots[E\cdots E]\cdots D\cdots[F\cdots F]\cdots])_n$ (Au(4)Au(5)Au(5)[c] 110.515(15)°, Au(5)Au(4)Au(6) 138.516(12)°, Au(4)-Au(6)Au(6)[d] 129.424(15)°; Au(4)–Au(5) 4.9410(8) Å, and Au(4)–Au(6) 4.4321(7) Å). To build the discussed

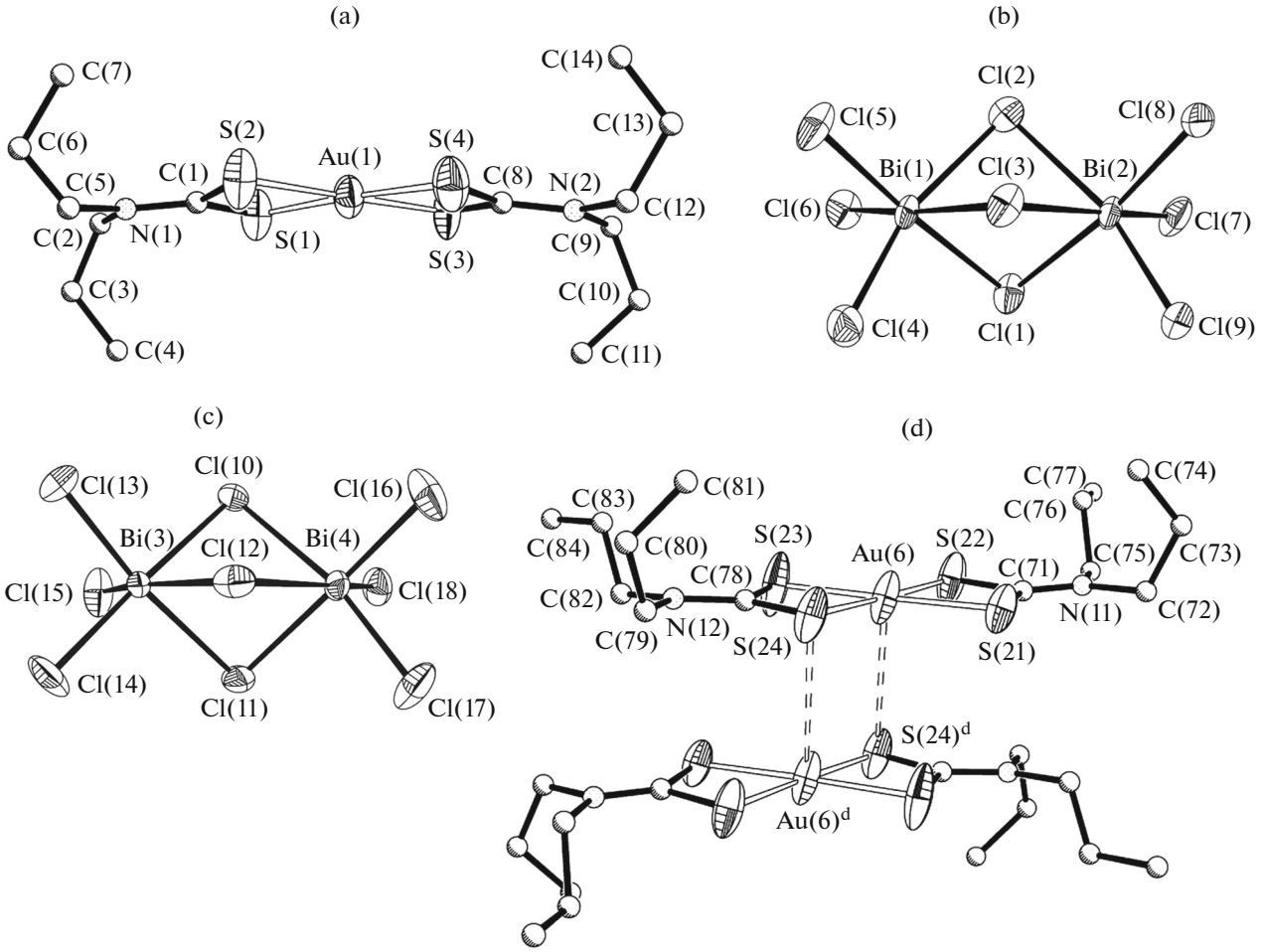

Fig. 2. Structural units of complex **II**: (a) mononuclear cation A $[Au\{S_2CN(C_3H_7)_2\}_2]^+$, (b, c) isomeric binuclear bismuth anions $[Bi_2Cl_9]^{3-}$, and (d) binuclear cation [E···E] $[Au_2\{S_2CN(C_3H_7)_2\}_4]^{2+}$. Secondary bonds Au···S are shown by double dashed lines. Ellipsoids of 50% probability.

supramolecular cation-cationic chains, mononuclear cations A and D enter the interdimer volume by the interacting moiety only and in such a way that their bisector axes C–Au–C are oriented relative to the bisector axes of the adjacent cations (in the composition of the binuclear aggregates) at the angle close to 90°. The planes of the $[AuS_4]$ chromophores of mononuclear cations A/D and cations B, C/E, and F in the adjacent dimers [B···C]/[E···E], and [F···F] form angles of 48.06(7)°, 44.26(7)°/46.93(9)°, and 44.33(9)°, respectively. In the both chains, the gold atoms of the binuclear cations form distorted octahedral $[AuS_6]$ chromophores, whereas the $[AuS_4]$ chromophores of the gold atoms are retained in the mononuclear cations.

The projection of the crystal structure on the *xz* plane (Fig. 4) reflects the "chess" order of alternation of the supramolecular cation-cationic polymer chains and isomeric binuclear bismuth anions. Each chain is isolated by the isomeric binuclear bismuth anions from four sides, and the stacks of the bismuth anions adjoin, in turn, with four polymer chains. Cation-anionic interactions of the nonvalent type take place between the binuclear bismuth(III) anions and polymer chains: secondary bonds Cl···S[2] [35, p. 266], whose formation involves four terminal chlorine atoms of each isomeric anion (three from one side of the anion and one from another side) and sulfur atoms in the binuclear cations $[Au_2\{S_2CN(C_3H_7)_2\}_4]^{2+}$. Each isomeric dibismuth anion participates in binding of two chains of the same type. The $[Bi_2Cl_9]^{3-}$ anions including Bi(1) and Bi(2) interact with the binuclear

[2] Cation-anionic interactions of this type were observed earlier for the formation of supramolecular structures of the heteronuclear complexes Au(III)–Zn [36] and Au(III)–Fe(III) [37].

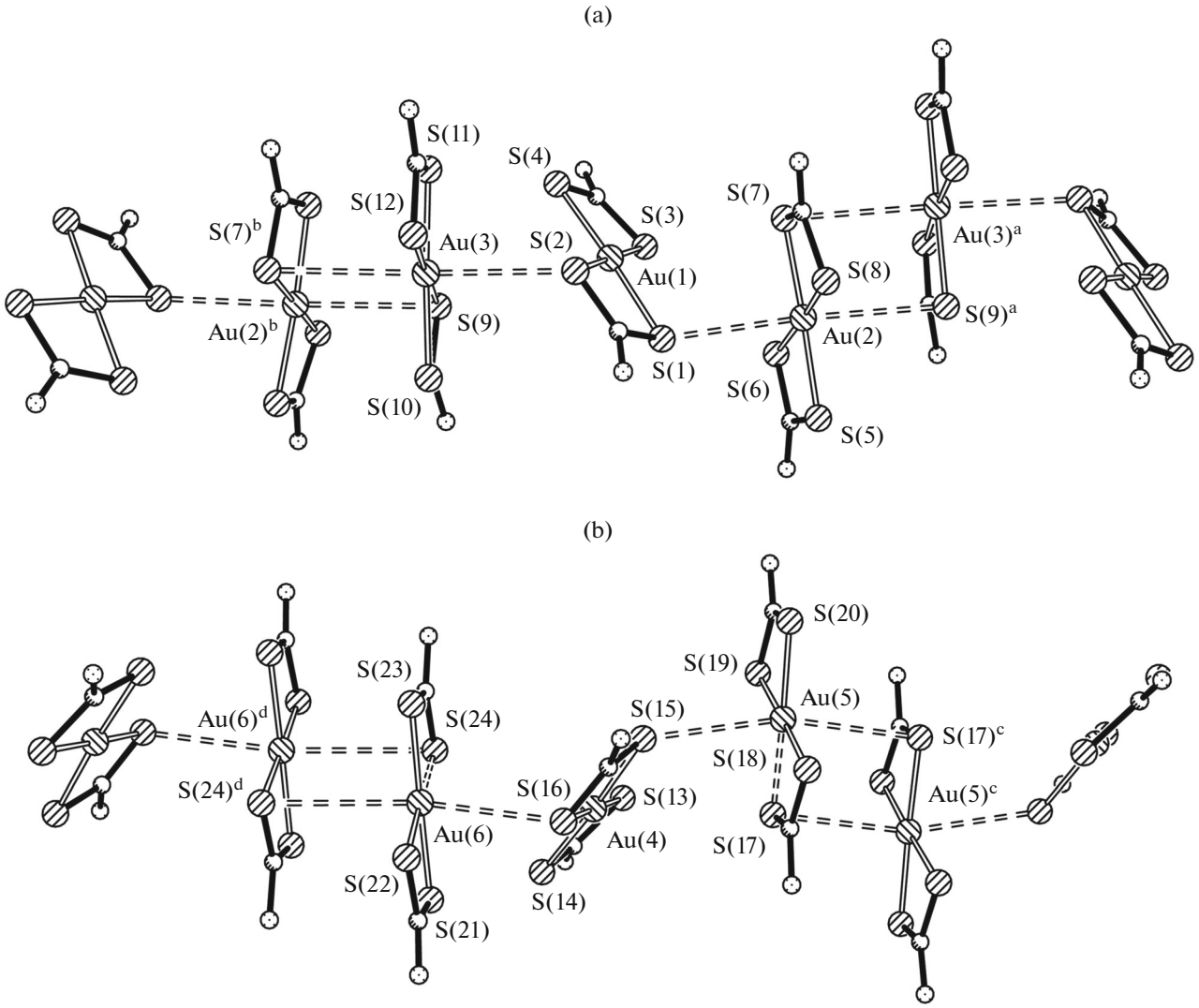

Fig. 3. Structural fragments of supramolecular polymer chains of two types: (a) $(\cdots A\cdots[B\cdots C]\cdots A\cdots[B\cdots C]\cdots)_n$ and (b) $(\cdots D\cdots[F\cdots F]\cdots D\cdots[E\cdots E]\cdots)_n$ built by isomeric complex cations A–F of the composition $[Au\{S_2CN(C_3H_7)_2\}_2]^+$. Secondary bonds Au···S are shown by double dashed lines; alkyl substituents are omitted.

cations [B···C] in the chains of the first type, and the anions with the Bi(3) and Bi(4) atoms join the chains of the second type including binuclear cations [E···E] and [F···F]. The anions discussed interact with the chains nonsymmetrically. Each isomeric anion forms with one of the chains one but the strongest secondary bond Cl···S: Cl(6)···S(12) (3.334 Å) and Cl(14)···S(20) (3.339 Å) (for comparison, the sum of the van der Waals radii of chlorine and sulfur atoms is 3.55 Å [33]). For the interaction with the second chain, the each isomeric anion presents three chlorine atoms (at another side of the anion) to form a set of less strong Cl···S bonds: 3.373–3.541 and 3.434–3.530 Å (Table 2).

It is important that the earlier described solvated form of complex **II** ($[Au\{S_2CN(C_3H_7)_2\}_2]_3[Bi_2Cl_9] \cdot 1/2OC(CH_3)_2 \cdot 1/2HCl)_n$ [23] is characterized by the absence of isomeric forms of anions $[Bi_2Cl_9]^{3-}$ and a basically different mode of supramolecular self-organization in the cationic moiety. Its structure contains four isomeric gold(III) cations involved in the construction of cationic triads $[Au_3\{S_2CN(C_3H_7)_2\}_6]^{3+}$ of two types differed in the character of internal binding. Direct aurophilic contacts Au···Au occurring between the discussed triads result in the formation of a supramolecular chain of the $(\cdots[C\cdots A\cdots C]\cdots[D\cdots B\cdots D]\cdots)_n$ type. Thus, the solvation of compound **II** is accompanied by a decrease in the number of isomeric forms of

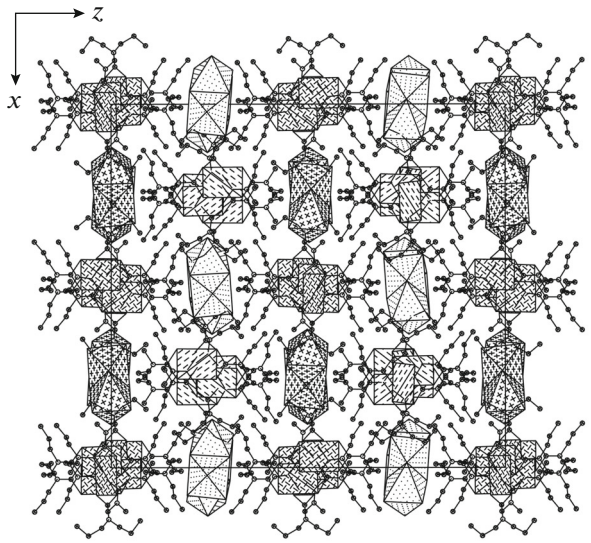

Fig. 4. Projection of the structure of compound **II** on the *xz* plane. Supramolecular cation-cationic chains are oriented along the *y* axis. In the polyhedral representation, polymer chains including cations Au(1)–Au(3) are designated by dash lines, chains with cations Au(4)–Au(6) are designated by intersecting dash lines, and binuclear anions Bi(1)–Bi(2) and Bi(3)–Bi(4) are shown by dots and daggers, respectively.

complex cations and anions and a change in the mode of supramolecular structure building.

The thermal behavior of complexes **I** and **II** was studied by the STA method in an argon atmosphere (parallel detection of TG and DSC curves). Compounds **I** and **II** are thermally stable to 193 and 152°C, respectively. The onset of a significant mass loss by compound **I** is detected by the TG curve (Fig. 5*a*) only after sample melting. The main mass loss (62.3%) falls on the steeply descending region of the TG curve in a range of 270–320°C (the maximum rate of mass loss is observed at 311.2°C). The formally one-stage process reflects the intensive thermolysis of complex **I** with the formation of Bi_2S_3 as the major final substance, and the subsequent flat region is caused by the smooth desorption of volatile thermolysis products. After the end of the process (at 550°C), the residual weight is 35.3%, which somewhat exceeds the calculated value for Bi_2S_3 (34.84%).

The DSC curve of compound **I** (Fig. 5*b*) in the low-temperature range (still before the onset of mass loss) exhibits two lowly intense endothermic effects with extremes at 144.9 and 162.7°C. The first irreversible endothermic effect indicates the phase transition in the substance to achieving the melting point. It is shown by independent measurements that the second endothermic effect is caused by sample melting (mp = 152–155°C); the extrapolated mp is 154.3°C. In the region falling on the steeply descending region of the TG curve, the DSC curve includes three weakly pronounced thermal effects (with extremes at 285.7, 311.0, and 315.6°C), indicating a complicated character of the formally one-stage thermolysis of complex **I**.

After the crucible was opened, a porous black substance with fragments of finest gray particles with metallic luster was observed. Scanning electron microscopy was used to refine the phase composition and chemical element distribution in the residue. The studied substance is mainly presented by plates 1.3–5.0 μm long collected into batches and by irregular particles (2.5–6.7 μm) (Fig. 6a). In addition, an impurity of larger round aggregates (16.3–31.0 μm) with traces of melting (Fig. 6b) was observed. The energy dispersive spectra show the presence of Bi, S, and C in the first case (Fig. 6a') and the presence of Bi and C in the second case (Fig. 6b'). Thus, the residual substance is Bi_2S_3 with an impurity of reduced metallic bismuth and elemental carbon. The presence of carbon in the residue after the pyrolysis of the bismuth complexes $[Bi(S_2CNR_2)_3]$ ($R = C_2H_5$; $R_2 = (CH_2)_5$, $(CH_2)_4O$) in an inert nitrogen atmosphere has previously been observed [38, 39]. In turn, the presence of metallic bismuth can be explained by the partial reduction of Bi_2S_3 with carbon and hydrogen during pyrolysis [40].

The region of the TG curve (132.0–613.0°C) reflecting the main mass loss during the thermolysis of complex **II** (62.3%) is presented by four weakly pronounced steps (Fig. 7*a*), the rate of mass loss on which decreases consequently with temperature. The first step (132.0–244.0°C) is due to the dissociation of one of the PDtc ligand in each of three complex cations $[Au\{S_2CN(C_3H_7)_2\}_2]^+$: the experimentally detected mass loss (22.3%) somewhat exceeds the calculated value (22.17%). The mass loss is 26.8% in the second step (244.0–322.0°C), which indicates that the thermolysis of the substance with respect to cation is completed (with gold reduction to the elemental state) and the simultaneous involvement of the $[Bi_2Cl_9]^{3-}$ anion in the process with the liberation of $BiCl_3$ (calcd. 26.63%). However, in the third step (322.0–415.0°C) related to the evaporation of $BiCl_3$ (mp = 234°C, bp = 440°C [41]), the mass loss (9.9%) composes only a relatively small portion of the expected value (calcd. 26.43%). It follows from this that a large portion of bismuth(III) transforms into Bi_2S_3[3] during the thermolysis of compound **II**. After the complete evaporation of $BiCl_3$,[4] the final desorption of volatiles (3.4%), including those accompanying the formation of Bi_2S_3,

[3] The formation of metal sulfides upon the thermolysis of the complexes including the sulfur-containing ligands was substantiated from the thermodynamic point of view [42].

[4] The evaporation of $BiCl_3$ was studied for samples of the compact substance. A significant mass loss begins from sample melting, the evaporation region lies in a range of 234.0–415.0°C, and the maximum rate of mass loss falls on 376.6°C.

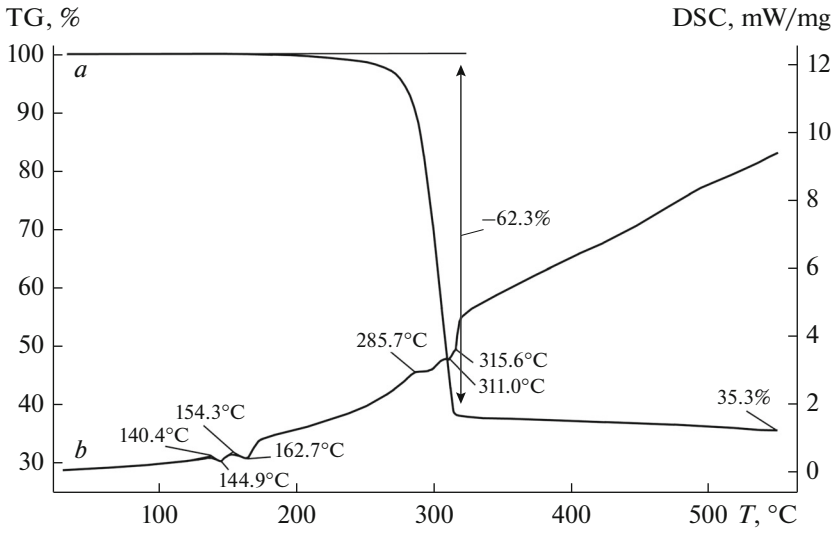

Fig. 5. (*a*) TG and (*b*) DSC curves for complex **I**.

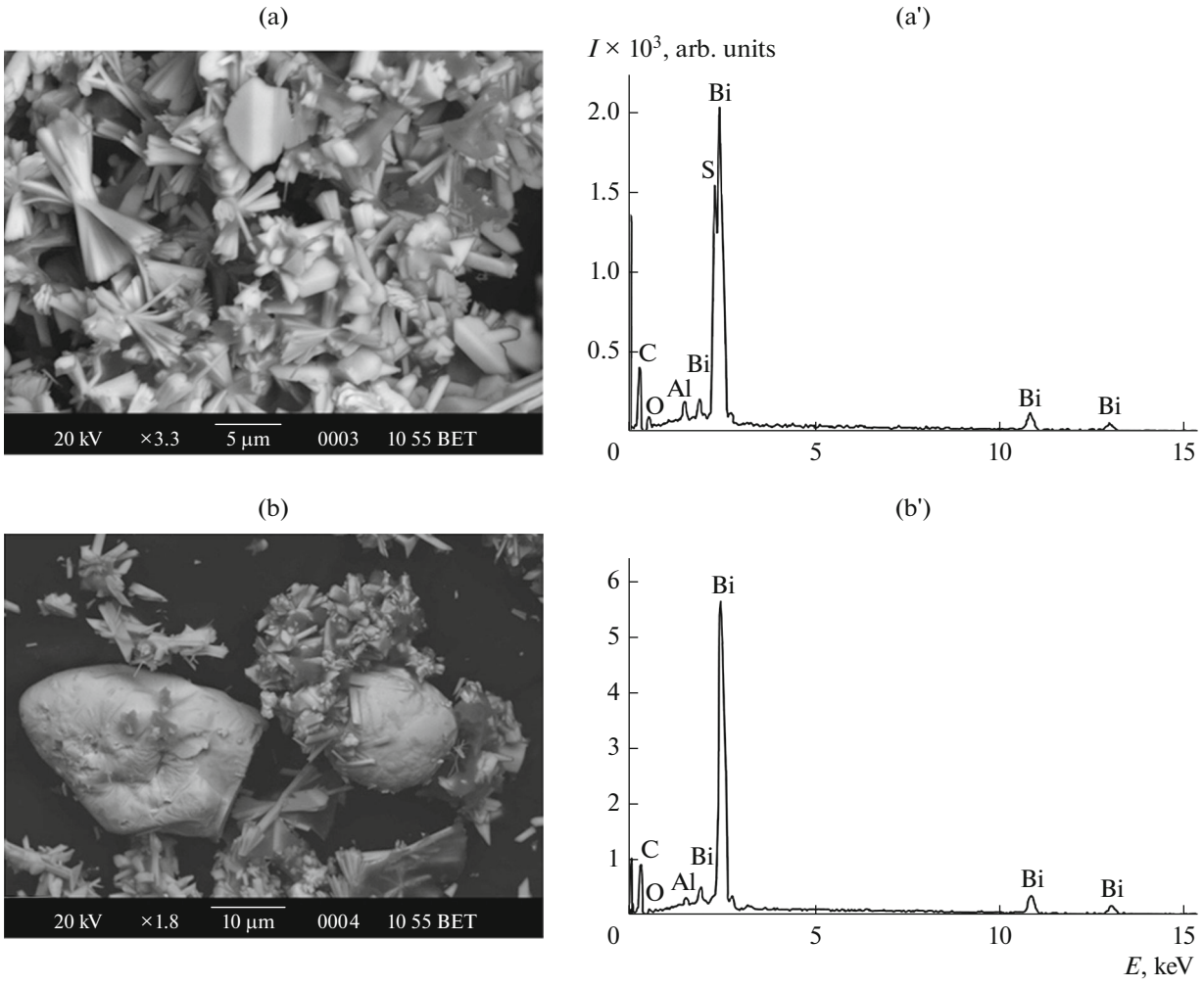

Fig. 6. Particle size and shape of (a) Bi_2S_3, (b) reduced metallic bismuth, and (a', b') their energy dispersive spectra, respectively.

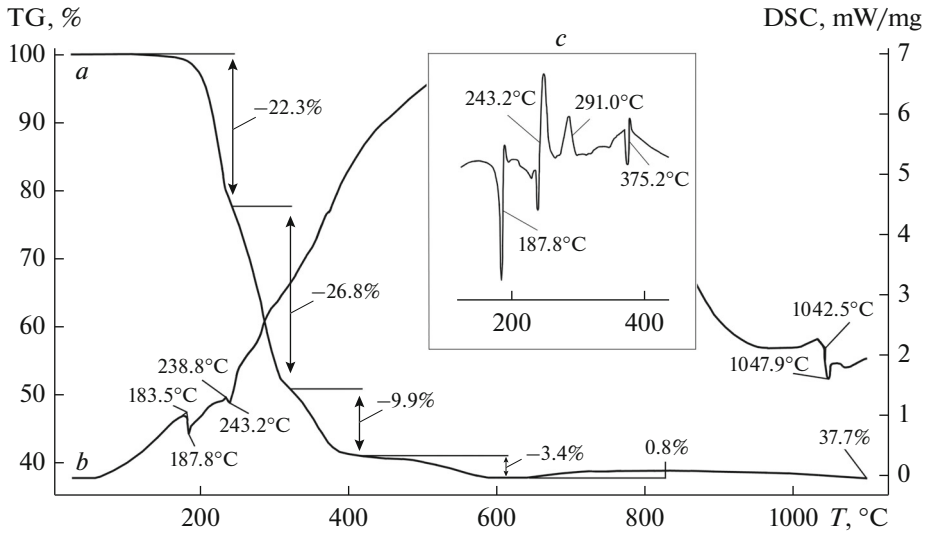

Fig. 7. (*a*) TG and (*b*) DSC curves for complex **II**. (*c*) First derivatives of thermal effects in the low-temperature DSC range: the middle of each line coincides with the extreme point of the corresponding thermal effect.

is observed in a range of 415.0–613.0°C (fourth step), and the weight of the residue reaches a minimum value of 37.7%.

Subtracting the weight of reduced gold (calcd. 24.77%) from the last value, one can easily determine the weight of the formed Bi_2S_3 (12.9%), which is 15.8% (based on $BiCl_3$) of the initial weight of compound **II**. It follows from this that the total weight of the formed $BiCl_3$ is 10.6% and its evaporation begins long before 322.0°C (lowest boundary of the third step). This conclusion is confirmed by the experimentally established range (234.0–415.0°C) of evaporation of compact $BiCl_3$. Thus, it follows from the complete calculation of the TG curve in a range of 132.0–613.0°C that the smaller portion of bismuth (40.1%) is isolated in the form of $BiCl_3$, whereas the larger portion (59.9%) transforms into Bi_2S_3.

In the high-temperature range beginning from 640°C, the TG curve of compound **II** detects a minor mass increase of 0.8%, which is explained by the oxidation of Bi_2S_3 with oxygen present in argon to $(BiO)_2SO_4$ [43] (calcd. 0.80%). As the temperature increases, $(BiO)_2SO_4$ dissociates to form Bi_2O_3, which is accompanied by a smooth decrease in the weight of the residue again to 37.7%. However, it is seen from the run of the TG curve (Fig. 7*a*) that at 1100°C the weight of the residue is not yet stabilized and the desorption of volatile products of the dissociation of bismuthyl sulfate is not completed. This is also favored by the calculation data: for the complete removal of volatile products of $(BiO)_2SO_4$ decomposition (13.7%) and Bi_2O_3 formation (11.7%), the mass loss should be 2.0% to which the final weight of the residue equal to 36.5% corresponds.

The DSC curve in the low-temperature range (Fig. 7*b*) is presented by several weakly pronounced thermal effects, and the differential approach was used to reveal them more distinctly (Fig. 7*c*). The first endothermic effect with an extreme at 187.8°C is related to the melting of compound **II**: the extrapolated mp is 183.5°C. The melting of compound **II** was established in a range of 184–187°C by the independent determination. The second endothermic effect with an extreme at 243.2°C is caused by the mass loss at the first TG step: the extrapolated temperature of the process (238.8°C) corresponds to the maximum rate of mass loss. The exothermic effect with an extreme at 291.0°C was attributed to the crystallization (isolation in the solid phase) of formed Bi_2S_3. The third endothermic effect with an extreme at 375.2°C is projected to the fourth step of the TG curve and, hence, reflects the evaporation of $BiCl_3$. The endothermic effect in the high-temperature range (with an extreme at 1047.9°C) is caused by melting of reduced gold: the extrapolated mp is 1042.5°C. This value (substantially underestimated compared to the reference mp of gold: 1064.18°C [41]) can be explained by an impurity of reduced metallic bismuth. After the end of thermolysis, the bottom of the opened crucible is covered by finest gold balls and lemon-yellow spots of a finely dispersed crystalline thin coating of Bi_2O_3.

ACKNOWLEDGMENTS

This work was supported in part by the Presidium of the Far East Branch of the Russian Academy of Sciences (project no. 15-I-3-001).

REFERENCES

1. de Carvalho, H.G. and de Araújo Penna, M., *Lett. Nuovo Cimento*, 1972, vol. 3, no. 18, p. 720.
2. de Marcillac, P., Coron, N., Dambier, G., et al., *Nature*, 2003, vol. 422, no. 6934, p. 876.
3. Li, H., Lai, C.S., Wu, J., et al., *J. Inorg. Biochem.*, 2007, vol. 101, no. 5, p. 809.
4. Ishak, D.H.A., Ooi, K.K., Ang, K.-P., et al., *J. Inorg. Biochem.*, 2014, vol. 130, p. 38.
5. Salvador, J.A.R., Figueiredo, S.A.C., Pinto, R.M.A., and Silvestre, S.M., *Future Med. Chem.*, 2012, vol. 4, no. 11, p. 1495.
6. Guo, Y.-C., Ma, Q.-G., Chen, S.-Y., et al., *Chin. J. Struct. Chem.*, 2015, vol. 34, no. 7, p. 1028.
7. Ozturk, I.I., Banti, C.N., Kourkoumelis, N., et al., *Polyhedron*, 2014, vol. 67, p. 89.
8. Arda, M., Ozturk, I.I., Banti, C.N., et al., *RSC Adv.*, 2016, vol. 6, p. 29026.
9. Chauhan, H.P.S., Joshi, S., and Carpenter, J., *J. Therm. Anal. Calorim.*, 2016, vol. 124, no. 1, p. 117.
10. Tamilvanan, S., Gurumoorthy, G., Thirumaran, S., and Ciattini, S., *Polyhedron*, 2017, vol. 121, p. 70.
11. Ariza-Roldán, A.O., López-Cardoso, E.M., Rosas-Valdez, M.E., et al., *Polyhedron*, 2017, vol. 134, p. 221.
12. Nomura, R., Kanaya, K., and Matsuda, H., *Bull. Chem. Soc. Jpn*., 1989, vol. 62, no. 3, p. 939.
13. Zhang, H., Huang, J., Zhou, X., and Zhong, X., *Inorg. Chem.*, 2011, vol. 50, no. 16, p. 7729.
14. Kun, W.N., Mlowe, S., Nyamen, L.D., et al., *Chem. Eur. J.*, 2016, vol. 22, no. 37, p. 13127.
15. Sivasekar, S., Ramalingam, K., Rizzoli, C., and Alexander, N., *Inorg. Chim. Acta*, 2014, vol. 419, p. 82.
16. Cabrita, J.F., Ferreira, V.C., and Monteiro, O.C., *Electrochim. Acta*, 2014, vol. 135, p. 121.
17. Abdullah, N.H., Zainal, Z., Silong, S., et al., *Thermochim. Acta*, 2016, vol. 632, p. 37.
18. Lai, C.S. and Tiekink, E.R.T., *Z. Kristallogr.*, 2007, vol. 222, no. 10, p. 532.
19. Ivanov, A.V., Egorova, I.V., Ivanov, M.A., et al., *Dokl. Phys. Chem.*, 2014, vol. 454, no. 1, p. 16.
20. Gowda, V., Sarma, B., Laitinen, R.S., et al., *Polyhedron*, 2017, vol. 129, p. 123.
21. Sun, R.-Z., Guo, Y.-C., Liu, W.-M., et al., *Chin. J. Struct. Chem.*, 2012, vol. 31, no. 5, p. 655.
22. Zaeva, A.S., Ivanov, A.V., Gerasimenko, A.V., and Sergienko, V.I., *Russ. J. Inorg. Chem.*, 2015, vol. 60, no. 2, p. 203. doi 10.1134/S0036023615020229
23. Zaeva, A.S., Ivanov, A.V., and Gerasimenko, A.V., *Russ. J. Coord. Chem.*, 2015, vol. 41, no. 10, p. 644. doi 10.1134/S1070328415090109
24. Byr'ko, V.M., *Ditiokarbamaty*, Moscow: Nauka, 1984.
25. Pines, A., Gibby, M.G., and Waugh, J.S., *J. Chem. Phys.*, 1972, vol. 56, no. 4, p. 1776.
26. *APEX2*, Madison: Bruker AXS Inc., 2010.
27. Sheldrick, G.M., *Acta Crystallogr., Sect. A: Found Crystallogr.*, 2008, vol. 64, no. 1, p. 112.
28. Fabretti, A.C., Forghieri, F., Giusti, A., et al., *Spectrochim. Acta, Part A*, 1984, vol. 40, no. 4, p. 343.
29. Yin, H., Li, F., and Wang, D., *J. Coord. Chem.*, 2007, vol. 60, no. 11, p. 1133.
30. Jaschinski, B., Blachnik, R., Pawlak, R., and Reuter, H., *Z. Kristallogr. NCS*, 1998, vol. 213, nos. 1–4, p. 541.
31. Savilov, S., Kloo, L., Kuznetsov, A., et al., *Z. Anorg. Allg. Chem.*, 2003, vol. 629, no. 14, p. 2525.
32. Gerasimenko, A.V., Karaseva, E.T., and Polishchuk, A.V., *Acta Crystallogr., Sect. E: Struct. Rep. Online*, 2008, vol. 64, no. 2, p. m378.
33. Winter, M., The Periodic Table of the Elements by Web Elements (accessed January 2010). http://www.webelements.com.
34. Alcock, N.W., *Adv. Inorg. Chem. Radiochem.*, 1972, vol. 15, no. 1, p. 1.
35. Haiduc, I. and Edelmann, F.T., *Supramolecular Organometallic Chemistry*, Wiley-VCH, 1999.
36. Loseva, O.V. and Ivanov, A.V., *Russ. J. Inorg. Chem.*, 2014, vol. 59, no. 12, p. 1491. doi 10.1134/S0036023614120146
37. Ivanov, A.V., Loseva, O.V., Rodina, T.A., et al., *Russ. J. Coord. Chem.*, 2016, vol. 42, no. 2, p. 104. doi 10.1134/S1070328416020032
38. Lalia-Kantouri, M., Christofides, A., and Manoussakis, G.E., *J. Therm. Anal. Calorim.*, 1984, vol. 29, no. 2, p. 279.
39. Lalia-Kantouri, M. and Manoussakis, G.E., *J. Therm. Anal. Calorim.*, 1984, vol. 29, no. 5, p. 1151.
40. Ripan, R. and Ceteanu, I., *Neorganicheskaya khimiya. T. 1. Khimiya metallov*, Spitsin, V.I., Kolli, I.D., Eds., Moscow: Mir, 1971.
41. Lidin, R.A., Andreeva, L.L., and Molochko, V.A., *Konstanty neorganicheskikh veshchestv: spravochnik* (Characteristics of Inorganic Compounds. A Handbook), Moscow: Drofa, 2008.
42. Razuvaev, G.A., Almazov, G.V., Domrachev, G.A., et al., *Dokl. Akad. Nauk SSSR*, 1987, vol. 294, no. 1, p. 141.
43. Larionov, S.V., Mikhalin, I.N., Glinskaya, L.A., et al., *Russ. J. Inorg. Chem.,* 2004, vol. 49, no. 3, p. 331.

Translated by E. Yablonskaya